1.1. Overview and principles of powder diffraction

R. E. Dinnebier and S. J. L. Billinge

1.1.1. Information content of a powder pattern

The structures of real materials comprise not only the crystal structure – the time- and space-averaged periodic configuration of atoms on an idealized periodic lattice – but also the microstructure, which is caused by imperfections, dislocations and all kinds of disorder. The microstructure is often responsible for interesting properties of the material. A powder diffraction pattern contains a wealth of information about this microstructure in addition to the average crystal structure, as shown schematically in Fig. 1.1.1.

At each stage of a powder diffraction study, great effort and ingenuity are needed to find the optimal experimental conditions and to understand and analyse the resulting line shapes and signals. As experimental equipment, theoretical understanding and computational tools have improved, it has become possible to tap into the rich information content of the line peak shapes and diffuse background of a typical powder diffraction pattern, yielding unprecedented information about real materials for materials scientists, chemists, physicists, earth scientists and engineers. For example, in the modern practice of whole-pattern modelling, the line profile is calculated from first principles, taking into account all aspects of the state of the sample, such as particle-size distributions, inhomogeneous strains and texture, as well as the experimental setup and aberrations. There is a useful feedback effect in that better profile descriptions result in more accurate determinations of the intensities of the Bragg peaks, which is important to extract accurate structural information (Bragg peaks are introduced in detail in the next section). Similarly, great progress has been made in the extraction of information from the diffuse signal that used to be called the 'background'. Rather than fitting the background using arbitrary fitting parameters, as is done in a traditional Rietveld refinement, careful corrections can be made for experimental effects such as Compton scattering, fluorescence, multiple scattering and scattering from sample environments. The resulting 'background' beneath and between the Bragg peaks of the corrected data is information-rich diffuse scattering from the sample, which contains information about the local structure and how it deviates from the average crystal structure in the form of defects and correlated lattice dynamics (phonons). Total-scattering methods that include both the Bragg and diffuse scattering are only now being fully appreciated, with quantitative analyses being carried out in real space using the atomic pair distribution function (PDF) method, and in reciprocal space with Monte Carlo simulated-annealing-type modelling based on the Debye equation.

In this introductory chapter, the basic physics behind the observation of a powder diffraction pattern is described. In accordance with the scheme in Fig. 1.1.1, the information in a powder diffraction pattern can be described by the Bragg-peak positions, the peak profile, the Bragg-peak intensities and the non-Bragg-scattering contributions to the background. After describing the fundamentals of scattering by a crystalline powder, the chapter is organized such that each of the paths illustrated in Fig. 1.1.1 is followed and described in an introductory way. Detailed descriptions of the state of the art in the kinds of studies covered in Fig. 1.1.1 can be found in following chapters, but here we discuss each aspect of powder diffraction in turn, giving a high-level overview of what information is available from powder diffraction as well as explaining the fundamental origin of the features containing that information. We do not attempt to review applications of the different kinds of studies, leaving that to the following chapters.

In this chapter we have drawn heavily on information within three textbooks (Dinnebier & Billinge, 2008; Mittemeijer & Welzel, 2012; Egami & Billinge, 2013) and references therein.

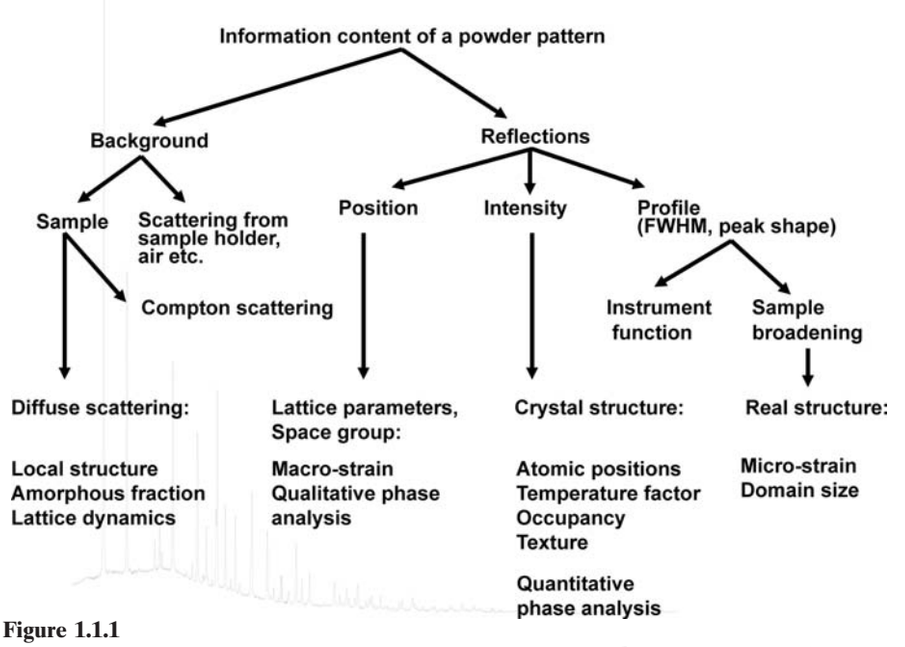

Figure 1.1.1
Schematic picture of the information content of a powder pattern. [Reproduced from Dinnebier & Billinge (2008) with permission from the Royal Society of Chemistry.]

1.1.2. The peak position

1.1.2.1. *The Bragg equation derived*

The easiest way to understand the structural information contained in powder diffraction, and historically one of the first ways in which diffraction was described, is *via* the well known Bragg equation (Bragg, 1913), which describes the principle of X-ray diffraction in terms of the reflection of X-rays by sets of lattice planes.

To understand the concept of a lattice plane, first imagine a three-dimensional periodic lattice of points, for example the corners of an array of cubes stacked in three dimensions. We can imagine a particular plane through the lattice by placing each layer of the stack of cubes on a tray: the tray then defines a lattice plane. Now imagine making the tray thinner and thinner until it

is infinitely thin, but still goes through the same set of points (the cube corners). What we see is that there is not just a single plane, but a series of equivalent planes: for example, between the top and second layers, the second and third layers, and so on. Each plane is parallel to the others and subsequent planes are separated by the same distance (the height of the cube). This is a set of lattice planes. We can also envisage inserting the trays in other ways. For example, we could place the trays vertically rather than horizontally and running from the left side to the right side of the stack of cubes, or alternatively running from the front of the stack to the back of the stack. Each of these is a different set of lattice planes (Fig. 1.1.2), although in this case they have the same layer spacing, or periodicity. If we were able to insert the tray at different angles to the cubes, for example at 45°, we could find other sets of parallel planes that, when we force them to go through some well defined subset of the points defining the lattice, will have well defined layer spacings or periodicities. Bragg's law showed that the diffraction pattern could be understood in terms of X-rays reflecting specularly off subsequent planes in each of these sets of planes and emerging in phase. (In reality, the actual effect is not specular reflection of light from an abstract plane, but a diffraction effect. However, the combination of diffraction and periodicity results in a selection rule that intense scattering only occurs when this particular specular-reflection condition holds.)

There are actually an infinite number of lattice planes in an infinite lattice, and it is important to have a way of labelling them, which is commonly done using the triplet of indices *hkl*, called Miller indices, where h, k and l are integers, and the separation of the planes is denoted by the distance d_{hkl}. When h, k and l have small values the planes are said to be 'low-order' planes. Low-order planes have the largest interplanar separations, and for a particular symmetry of the lattice there is a direct relationship between the Miller indices and d_{hkl}.

The Bragg equation gives the condition that must hold for specular reflection from subsequent planes in a set to be perfectly in phase, as illustrated in Fig. 1.1.3. It is evident in Fig. 1.1.3 that the wave reflecting off the lower plane travels a longer distance (by PN before and NQ after reflection occurs) than the wave reflecting off the upper plane. The two waves are in phase, resulting in constructive interference, only when $\Delta = |\mathrm{PN}| + |\mathrm{NQ}|$ is a multiple $n = 0, 1, 2, \ldots$ of the wavelength λ,

$$\Delta = n\lambda. \tag{1.1.1}$$

In all other cases, destructive interference results, since it is always possible to find a deeper plane, p, for which the relation

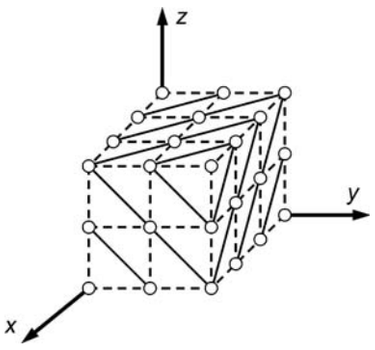

Figure 1.1.2
Schematic drawing of a set of parallel lattice planes (111) passing through all points of the cubic lattice.

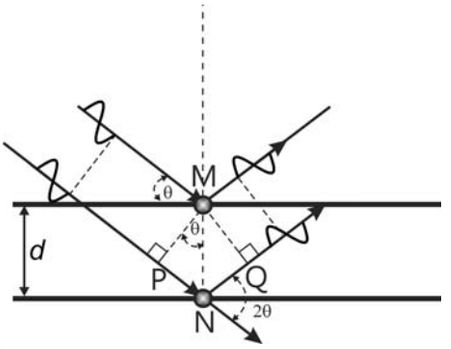

Figure 1.1.3
Illustration of the geometry used for the simplified derivation of Bragg's law. [Reproduced from Dinnebier & Billinge (2008) with permission from the Royal Society of Chemistry.]

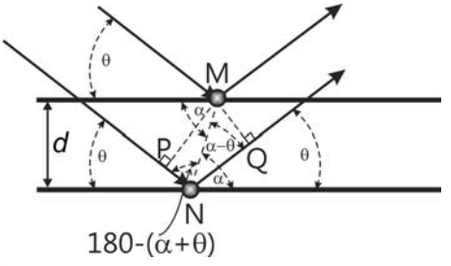

Figure 1.1.4
Illustration of the geometry in the general case where scattering takes place at the position of atoms in consecutive planes. [Reproduced from Dinnebier & Billinge (2008) with permission from the Royal Society of Chemistry.]

$p\Delta = n\lambda + 1/2$ exactly holds, giving rise to perfect destructive interference. Thus, when a narrow beam of X-rays impinges on a crystalline sample, sharp peaks in the intensity of the scattered X-rays are seen only at the angles for which equation (1.1.1) holds, with no intensity observed at other angles. As can easily be seen from Fig. 1.1.3, geometrically,

$$\Delta = 2d \sin\theta, \tag{1.1.2}$$

where d is the interplanar spacing of the parallel lattice planes and 2θ is the diffraction (or 'scattering') angle, the angle between the incoming and outgoing X-ray beams. The angle $\theta = 2\theta/2$ is often called the Bragg angle. Combining equations (1.1.1) and (1.1.2) we get

$$n\lambda = 2d \sin\theta, \tag{1.1.3}$$

which is the Bragg equation (Bragg, 1913).

This simplified derivation of the Bragg equation is often reproduced in textbooks. Although it leads to the correct solution, it has a serious drawback. In reality the X-rays are not reflected by planes, but are scattered by electrons bound to the atoms in the sample. The planes within a crystal are not like shiny optical mirrors, but contain discrete atoms separated by regions of much lower electron density and, in general, the atoms in one plane will not lie exactly above atoms in the plane below as implied by Fig. 1.1.3. How is it then that the simplified picture shown in Fig. 1.1.3 gives the correct result? A more general description shows that equation (1.1.3) is also valid if the atom in the lower lattice plane in Fig. 1.1.3 is shifted by an arbitrary amount within the plane (Fig. 1.1.4).

The phase shift can immediately be deduced from Fig. 1.1.4 as

$$\begin{aligned} n\lambda &= \mathrm{MN}\cos[180^\circ - (\alpha + \theta)] + \mathrm{MN}\cos(\alpha - \theta) \\ &= \mathrm{MN}[-\cos(\alpha + \theta) + \cos(\alpha - \theta)]. \end{aligned} \tag{1.1.4}$$

Using the standard trigonometric results

$$\cos(\alpha+\theta)=\cos\alpha\cos\theta-\sin\alpha\sin\theta,$$
$$\cos(\alpha-\theta)=\cos\alpha\cos\theta+\sin\alpha\sin\theta, \quad (1.1.5)$$

equation (1.1.4) becomes

$$n\lambda=\mathrm{MN}(2\sin\alpha\sin\theta) \quad (1.1.6)$$

with

$$d=\mathrm{MN}\sin\alpha, \quad (1.1.7)$$

which may be substituted to yield the Bragg equation:

$$n\lambda=2d\sin\theta. \quad (1.1.8)$$

The Bragg equation holds for any radiation or particle that is used to probe the structure of the sample: X-rays, neutrons or electrons. Another equivalent, and highly useful, form of the Bragg equation for the particular case of X-rays is

$$Ed=\frac{6.199}{\sin\theta}\ \text{with}\ \lambda=\frac{12.398}{E}, \quad (1.1.9)$$

where the energy E of the X-rays is in keV and λ is in ångströms.

The Bragg law results in narrow beams of high intensity that emerge from the crystal in specific directions given by the Bragg equation, resulting in sharp spots on the detector, and there is a one-to-one correspondence between these Bragg spots (often referred to as Bragg reflections) and each set of crystallographic planes. Each Bragg spot is therefore labelled with the same set of Miller indices, *hkl*, as the set of planes that gave rise to it.

It is possible to construct a 'reciprocal space' where the axes of the space are in units of inverse length. The reference coordinate frame of the reciprocal space is defined by a set of basis vectors whose directions are perpendicular to the plane normals of the (100), (010) and (100) planes of the crystal. Thus, a *point* in this reciprocal space corresponds to a *direction* in direct space and every allowed reflection according to the Bragg law is represented by a point in reciprocal space. The set of points arising from the Bragg law forms a lattice in reciprocal space, which is called the 'reciprocal lattice', and each single crystal has its own reciprocal lattice. [See *International Tables for Crystallography* Volume B (Shmueli, 2008) for more details.]

To derive the Bragg equation, we used an assumption of specular reflection, which is borne out by experiment: for a crystalline material, destructive interference eliminates scattered intensity in all directions except where equation (1.1.3) holds. Strictly this holds only for crystals that are infinite in extent and which the incident X-ray beam can penetrate without loss of intensity. This does not sound like a particularly good approximation, but in practice it holds rather well. Even a fairly low energy X-ray beam that only penetrates, say, a micrometre into the material will still probe ~10 000 atomic layers. The condition is not strictly obeyed in the presence of defects and disorder in the material. In such materials the Bragg peaks are modified in their position, their width and their shape, and there is also an additional component of the diffracted intensity that may be observed in all directions, away from reciprocal-lattice points, known as diffuse scattering.

1.1.2.2. *The Bragg equation from the reciprocal lattice*

Here we develop in more detail the mathematics of the reciprocal lattice. The reciprocal lattice has been adopted by crystallographers as a simple and convenient representation of the physics of diffraction by a crystal. It is an extremely useful tool for describing all kinds of diffraction phenomena occurring in powder diffraction.

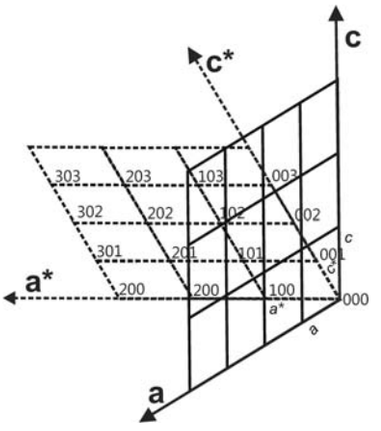

Figure 1.1.5
A two-dimensional monoclinic lattice and its corresponding reciprocal lattice. [Adapted from Dinnebier & Billinge (2008) with permission from the Royal Society of Chemistry.]

Consider a 'normal' crystal lattice with lattice vectors **a**, **b** and **c**, which have lengths a, b and c, respectively, and angles α between **b** and **c**, β between **a** and **c** and γ between **a** and **b**. The unit-cell volume is given by V. A second lattice with lattice parameters a^*, b^*, c^*, α^*, β^*, γ^* and unit-cell volume V^* with the same origin exists such that

$$\mathbf{a}\cdot\mathbf{b}^*=\mathbf{a}\cdot\mathbf{c}^*=\mathbf{b}\cdot\mathbf{c}^*=\mathbf{a}^*\cdot\mathbf{b}=\mathbf{a}^*\cdot\mathbf{c}=\mathbf{b}^*\cdot\mathbf{c}=0,$$
$$\mathbf{a}\cdot\mathbf{a}^*=\mathbf{b}\cdot\mathbf{b}^*=\mathbf{c}\cdot\mathbf{c}^*=1. \quad (1.1.10)$$

This is known as the reciprocal lattice[1] (Fig. 1.1.5), which exists in so-called reciprocal space. As mentioned above, we will see that it turns out that the points in the reciprocal lattice are related to the vectors defining the crystallographic plane normals. There is one point in the reciprocal lattice for each set of crystallographic planes, (*hkl*), separated by distance d_{hkl}, as discussed below. For now, just consider h, k and l to be integers that index a point in the reciprocal lattice. A reciprocal-lattice vector $\mathbf{h}_{hkl}$ is the vector from the origin of reciprocal space to the reciprocal-lattice point for the plane (*hkl*),

$$\mathbf{h}_{hkl}=h\mathbf{a}^*+k\mathbf{b}^*+l\mathbf{c}^*,\quad h,k,l\in\mathbb{Z}. \quad (1.1.11)$$

where $\mathbb{Z}$ is the set of all integers.

The length of the reciprocal basis vector $\mathbf{a}^*$ is defined according to

$$\mathbf{a}^*=x(\mathbf{b}\times\mathbf{c}), \quad (1.1.12)$$

where the scale factor x can easily be deduced, using equations (1.1.12) and (1.1.10), as

$$\mathbf{a}^*\cdot\mathbf{a}=x(\mathbf{b}\times\mathbf{c}\cdot\mathbf{a})=xV\Rightarrow x=\frac{1}{V}, \quad (1.1.13)$$

leading to

$$\mathbf{a}^*=\frac{1}{V}(\mathbf{b}\times\mathbf{c}),\quad \mathbf{b}^*=\frac{1}{V}(\mathbf{c}\times\mathbf{a}),\quad \mathbf{c}^*=\frac{1}{V}(\mathbf{a}\times\mathbf{b}) \quad (1.1.14)$$

and, *vice versa*,

[1] The reciprocal lattice is a commonly used construct in solid-state physics, but with a different normalization: $\mathbf{a}\cdot\mathbf{a}^*=2\pi$.

$$\mathbf{a} = \frac{1}{V^*}(\mathbf{b}^* \times \mathbf{c}^*), \quad \mathbf{b} = \frac{1}{V^*}(\mathbf{c}^* \times \mathbf{a}^*), \quad \mathbf{c} = \frac{1}{V^*}(\mathbf{a}^* \times \mathbf{b}^*). \tag{1.1.15}$$

The relationship between the reciprocal and the real lattice parameters expressed geometrically rather than in the vector formalism used above is

$$\begin{aligned} a^* &= \frac{bc\sin\alpha}{V}, \\ b^* &= \frac{ac\sin\beta}{V}, \\ c^* &= \frac{ab\sin\gamma}{V}, \\ \cos\alpha^* &= \frac{\cos\beta\cos\gamma - \cos\alpha}{\sin\beta\sin\gamma}, \\ \cos\beta^* &= \frac{\cos\alpha\cos\gamma - \cos\beta}{\sin\alpha\sin\gamma}, \\ \cos\gamma^* &= \frac{\cos\alpha\cos\beta - \cos\gamma}{\sin\alpha\sin\beta}, \\ V &= abc\sqrt{1 + 2\cos\alpha\cos\beta\cos\gamma - \cos^2\alpha - \cos^2\beta - \cos^2\gamma}. \end{aligned} \tag{1.1.16}$$

Equation (1.1.16) is the most general expression for non-orthogonal lattices. The expressions simplify considerably for higher-symmetry crystal systems.

We now re-derive Bragg's law using the vector notation introduced above (Fig. 1.1.6). The wave vectors of the incoming and outgoing beams are given by $\mathbf{s}_0$ and $\mathbf{s}$, respectively. They point in the direction of propagation of the wave and their length depends on λ. For elastic scattering (for which there is no change in wavelength on scattering), $\mathbf{s}_0$ and $\mathbf{s}$ have the same length.

We define the scattering vector as

$$\mathbf{h} = (\mathbf{s} - \mathbf{s}_0), \tag{1.1.17}$$

which for a specular reflection is always perpendicular to the scattering plane. The length of $\mathbf{h}$ is given by

$$\frac{h}{s} = 2\sin\theta. \tag{1.1.18}$$

Comparison with the formula for the Bragg equation (1.1.3),

$$\frac{n\lambda}{d} = 2\sin\theta, \tag{1.1.19}$$

gives

$$\frac{n\lambda}{d} = \frac{h}{s}. \tag{1.1.20}$$

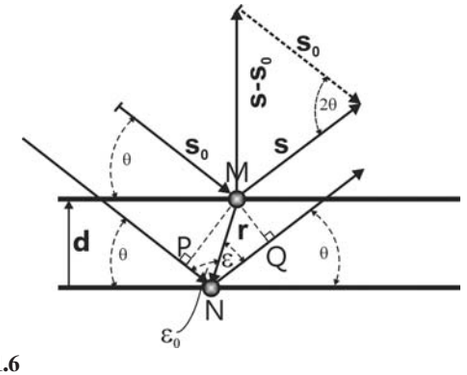

Figure 1.1.6
Illustration of the important wave and scattering vectors in the case of elastic Bragg scattering. [Reproduced from Dinnebier & Billinge (2008) with permission from the Royal Society of Chemistry.]

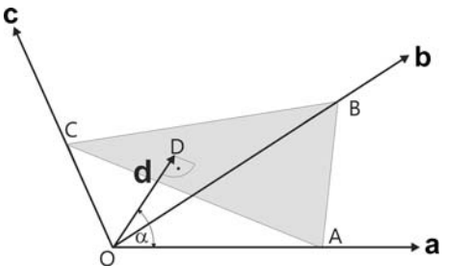

Figure 1.1.7
Geometrical description of a lattice plane in terms of real-space basis vectors. The arc and dot below the letter D indicate a right angle. [Reproduced from Dinnebier & Billinge (2008) with permission from the Royal Society of Chemistry.]

Setting the magnitude of $\mathbf{s}$ to $1/\lambda$, we get the Bragg equation in terms of the magnitude h of the scattering vector,

$$h = \frac{n}{d}. \tag{1.1.21}$$

This shows that diffraction occurs when the magnitude of the scattering vector is an integral number of reciprocal-lattice spacings $1/d$. We define a vector $\mathbf{d}^*$ perpendicular to the lattice planes with length $1/d$. Since $\mathbf{h}$ is perpendicular to the scattering plane, this leads to

$$\mathbf{h} = n\mathbf{d}^*. \tag{1.1.22}$$

Diffraction can occur at different scattering angles 2θ for the same crystallographic plane, giving the different orders n of diffraction. For simplicity, the number n will be incorporated in the indexing of the lattice planes, where

$$d^*_{nh,nk,nl} = nd^*_{hkl}, \tag{1.1.23}$$

e.g., $d^*_{222} = 2d^*_{111}$, and we get an alternative expression for Bragg's equation:

$$\mathbf{h} = \mathbf{d}^*_{hkl}. \tag{1.1.24}$$

The vector $\mathbf{d}^*_{hkl}$ points in a direction perpendicular to a real-space lattice plane. We would like to express this vector in terms of the reciprocal-space basis vectors $\mathbf{a}^*$, $\mathbf{b}^*$, $\mathbf{c}^*$.

First we define $\mathbf{d}_{hkl}$ in terms of the real-space basis vectors $\mathbf{a}$, $\mathbf{b}$, $\mathbf{c}$. Referring to Fig. 1.1.7, we can define

$$\mathbf{OA} = \frac{1}{h}\mathbf{a}, \quad \mathbf{OB} = \frac{1}{k}\mathbf{b}, \quad \mathbf{OC} = \frac{1}{l}\mathbf{c} \tag{1.1.25}$$

with h, k and l being integers, as required by the periodicity of the lattice.

The plane-normal vector $\mathbf{d}_{hkl}$ originates on one plane and terminates on the next parallel plane. Therefore, $\mathbf{OA}\cdot\mathbf{d} = (\mathrm{OA})d\cos\alpha$. From Fig. 1.1.7 we see that, geometrically, $(\mathrm{OA})\cos\alpha = d$. Substituting, we get $\mathbf{OA}\cdot\mathbf{d} = d^2$. Combining this with equation (1.1.25) leads to

$$\frac{1}{h}\mathbf{a}\cdot\mathbf{d} = d^2 \tag{1.1.26}$$

and consequently

$$h = \mathbf{a}\cdot\frac{\mathbf{d}}{d^2}, \quad k = \mathbf{b}\cdot\frac{\mathbf{d}}{d^2}, \quad l = \mathbf{c}\cdot\frac{\mathbf{d}}{d^2}. \tag{1.1.27}$$

By definition, h, k and l are divided by their largest common integer to be Miller indices. The vector $\mathbf{d}^*_{hkl}$, from Bragg's equation (1.1.24), points in the plane-normal direction parallel to $\mathbf{d}$ but with length $1/d$. We can now write $\mathbf{d}^*_{hkl}$ in terms of the

vector **d**:

$$\mathbf{d}^*_{hkl} = \frac{\mathbf{d}}{d^2}, \tag{1.1.28}$$

which gives

$$\mathbf{d}^*_{hkl} = \frac{\mathbf{d}_{hkl}}{d^2} = h\mathbf{a} + k\mathbf{b} + l\mathbf{c}, \tag{1.1.29}$$

or written in terms of the reciprocal basis

$$\mathbf{d}^*_{hkl} = h\mathbf{a}^* + k\mathbf{b}^* + l\mathbf{c}^*, \tag{1.1.30}$$

which was obtained using

$$\begin{aligned}\mathbf{d}^*_{hkl}\cdot\mathbf{a}^* &= h\mathbf{a}\cdot\mathbf{a}^* + k\mathbf{b}\cdot\mathbf{a}^* + l\mathbf{c}\cdot\mathbf{a}^* = h,\\ \mathbf{d}^*_{hkl}\cdot\mathbf{b}^* &= h\mathbf{a}\cdot\mathbf{b}^* + k\mathbf{b}\cdot\mathbf{b}^* + l\mathbf{c}\cdot\mathbf{b}^* = k,\\ \mathbf{d}^*_{hkl}\cdot\mathbf{c}^* &= h\mathbf{a}\cdot\mathbf{c}^* + k\mathbf{b}\cdot\mathbf{c}^* + l\mathbf{c}\cdot\mathbf{c}^* = l.\end{aligned} \tag{1.1.31}$$

Comparing equation (1.1.30) with equation (1.1.11) proves the identity of $\mathbf{d}^*_{hkl}$ and the reciprocal-lattice vector $\mathbf{h}_{hkl}$. Bragg's equation, (1.1.24), can be re-stated as

$$\mathbf{h} = \mathbf{h}_{hkl}. \tag{1.1.32}$$

In other words, diffraction occurs whenever the scattering vector **h** equals a reciprocal-lattice vector $\mathbf{h}_{hkl}$. This powerful result is visualized in the useful Ewald construction, which is described in Section 1.1.2.4.

Useful equivalent variations of the Bragg equation are

$$|\mathbf{h}| = \left|\mathbf{s} - \mathbf{s}_0\right| = \frac{2\sin\theta}{\lambda} = \frac{1}{d} \tag{1.1.33}$$

and

$$|\mathbf{Q}| = \frac{4\pi\sin\theta}{\lambda} = \frac{2\pi}{d}. \tag{1.1.34}$$

The vector **Q** is the physicist's equivalent of the crystallographer's **h**. The physical meaning of **Q** is the momentum transfer on scattering and it differs from the scattering vector **h** by a factor of 2π.

1.1.2.3. *The Bragg equation from the Laue equation*

Another approach for describing scattering from a material was first described by Laue (von Laue, 1912). The Laue equation can be derived by evaluating the phase relation between two wavefronts after hitting two scatterers that are separated by the vector **r**. The path-length difference $\Delta = |\mathrm{CD}| - |\mathrm{BA}|$ between the two scattered waves introduces a phase shift between the two outgoing waves (Fig. 1.1.8). From Fig. 1.1.8 one immediately sees that the path-length difference is given by

$$\Delta = r\cos\varepsilon - r\cos\varepsilon_0. \tag{1.1.35}$$

This path-length difference gives rise to a phase shift

$$\varphi = 2\pi\frac{\Delta}{\lambda} = 2\pi\left(\frac{r}{\lambda}\cos\varepsilon - \frac{r}{\lambda}\cos\varepsilon_0\right). \tag{1.1.36}$$

The term in parentheses is

$$\mathbf{s}\cdot\mathbf{r} - \mathbf{s_0}\cdot\mathbf{r} = (\mathbf{s} - \mathbf{s_0})\cdot\mathbf{r} = \mathbf{h}\cdot\mathbf{r}. \tag{1.1.37}$$

The amplitude of the scattered wave at a large distance away in the direction of the vector **s** is

$$A(\mathbf{h}) = \exp(2\pi i 0) + \exp(2\pi i\mathbf{h}\cdot\mathbf{r}) \tag{1.1.38}$$

When we generalize the idea laid out above to *n* scatterers, we get

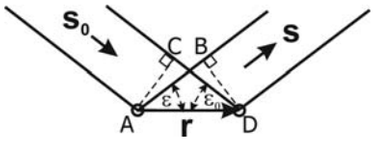

Figure 1.1.8
Scattering from an object consisting of two scatterers separated by **r**.

$$A(\mathbf{h}) = \sum_{j=1}^{n}\exp\left(2\pi i\mathbf{h}\cdot\mathbf{r}_j\right). \tag{1.1.39}$$

For simplicity, consider the case of an infinite one-dimensional crystal of scatterers that are equally spaced by distance a_i. In this case, $r_j = aj$ and

$$A(h) = \sum_{j=-\infty}^{\infty}\exp(2\pi i haj). \tag{1.1.40}$$

Using the definition for a periodic delta function,

$$\lim_{n\to\infty}\sum_{j=-n}^{n}\exp(2\pi i haj) = \sum_{k=-\infty}^{\infty}\delta(k - ha) \tag{1.1.41}$$

and

$$A(h) = \sum_{k=-\infty}^{\infty}\delta(k - ha), \tag{1.1.42}$$

which is a periodic array of delta functions at positions $h = k/a$. This means that sharp peaks of intensity will only appear when this expression holds, which are the reciprocal-lattice points. This is the same result as given by the Bragg equation (1.1.3) in one dimension. Extending to three dimensions, equations (1.1.40) and (1.1.42) become

$$\begin{aligned}A(\mathbf{h}) = &\sum_{j=-\infty}^{\infty}\exp\left(2\pi i(\mathbf{h}\cdot\hat{\mathbf{a}})aj\right)\sum_{k=-\infty}^{\infty}\exp\left(2\pi i(\mathbf{h}\cdot\hat{\mathbf{b}})bk\right)\\ &\times\sum_{l=-\infty}^{\infty}\exp\left(2\pi i(\mathbf{h}\cdot\hat{\mathbf{c}})cl\right),\end{aligned} \tag{1.1.43}$$

where $\hat{\mathbf{a}} = \mathbf{a}/a$, and

$$A(\mathbf{h}) = \sum_{\mu,\nu,\eta=-\infty}^{\infty}\delta[\mu - (\mathbf{h}\cdot\hat{\mathbf{a}})a]\delta[\nu - (\mathbf{h}\cdot\hat{\mathbf{b}})b]\delta[\eta - (\mathbf{h}\cdot\hat{\mathbf{c}})c]. \tag{1.1.44}$$

Equation (1.1.44) has the same meaning in three dimensions, where intensity appears only when all three delta functions are non-zero. This occurs for the conditions

$$\mathbf{h}\cdot\hat{\mathbf{a}} = \frac{\mu}{a},\ \ \mathbf{h}\cdot\hat{\mathbf{b}} = \frac{\nu}{b}\ \text{and}\ \mathbf{h}\cdot\hat{\mathbf{c}} = \frac{\eta}{c}, \tag{1.1.45}$$

where μ, ν and η are integers. From this follows

$$\mathbf{h}\cdot\mathbf{a} = \mu,\ \ \mathbf{h}\cdot\mathbf{b} = \nu\ \text{and}\ \mathbf{h}\cdot\mathbf{c} = \eta. \tag{1.1.46}$$

These conditions are met when

$$\mathbf{h} = \mu\mathbf{a}^* + \nu\mathbf{b}^* + \eta\mathbf{c}^* = \mathbf{d}^*_{\mu\nu\eta}. \tag{1.1.47}$$

This is exactly Bragg's equation in the form given in equation (1.1.30).

For practical purposes including the indexing of powder patterns and refinement of a structural model, given a set of lattice parameters *a*, *b*, *c*, α, β, γ, the positions for all possible reflections *hkl* can be calculated according to

$$\frac{1}{d_{hkl}} = \frac{1}{V}\left\{\left[h^2b^2c^2\sin^2\alpha + k^2a^2c^2\sin^2\beta + l^2a^2b^2\sin^2\gamma + 2hkabc^2(\cos\alpha\cos\beta - \cos\gamma) + 2kla^2bc(\cos\beta\cos\gamma - \cos\alpha) + 2hlab^2c(\cos\alpha\cos\gamma - \cos\beta)\right]\right\}^{1/2}, \quad (1.1.48)$$

for the triclinic case. Equation (1.1.48) simplifies considerably with symmetry to, for example,

$$\frac{1}{d_{hkl}} = \frac{\sqrt{h^2 + k^2 + l^2}}{a} \quad (1.1.49)$$

for the cubic case.

1.1.2.4. *The Ewald construction and Debye–Scherrer cones*

The Bragg equation shows that diffraction occurs when the scattering vector equals a reciprocal-lattice vector. The scattering vector depends on the geometry of the experiment, whereas the reciprocal-lattice vectors are determined by the orientation and the lattice parameters of the crystalline sample. Bragg's law shows the relationship between these vectors in a scattering experiment. Ewald developed a powerful geometric construction that combines these two concepts in an intuitive way (Ewald, 1921). A sphere of radius $1/\lambda$ is drawn following the recipe below. The Bragg equation is satisfied and diffraction occurs whenever a reciprocal-lattice point coincides with the surface of the sphere.

The recipe for constructing Ewald's sphere[2] is as follows (Fig. 1.1.9):

(1) Draw the incident wave vector $\mathbf{s}_0$. This points in the direction of the incident beam and has length $1/\lambda$.
(2) Draw a sphere centred on the tail of this vector with radius $1/\lambda$. The incident wave vector $\mathbf{s}_0$ defines the radius of the sphere. The scattered wave vector $\mathbf{s}$, also of length $1/\lambda$, points in the direction from the sample to the detector. This vector is also drawn starting from the centre of the sphere and also terminates at a point on the surface of the sphere. The scattering vector $\mathbf{h} = \mathbf{s} - \mathbf{s}_0$ completes the triangle from the tip of $\mathbf{s}$ to the tip of $\mathbf{s}_0$, both of which lie on the surface of the sphere. Thus the surface of the sphere defines the locus of points in reciprocal space where the scattering vector in our experiment may possibly lie.
(3) Draw the reciprocal lattice with the origin lying at the tip of $\mathbf{s}_0$.
(4) Find all the places on the surface of the sphere where reciprocal-lattice points lie. This gives the set of points in reciprocal space where the expression $\mathbf{h} = \mathbf{h}_{hkl}$ may possibly be satisfied in our experiment.

This construction places a reciprocal-lattice point at one end of $\mathbf{h}$. The other end of $\mathbf{h}$ lies on the surface of the sphere by definition. Thus, Bragg's law is only satisfied when another reciprocal-lattice point coincides with the surface of the sphere. Diffraction can be envisaged as beams of X-rays emanating from the sample in these directions. In order to detect the intensity of these diffracted beams, one simply moves the detector to the right position. Any vector between two reciprocal-lattice points has the potential to produce a Bragg peak. The Ewald-sphere construction indicates which of these possible reflections are experimentally accessible.

[2] For practical reasons, plots of the Ewald 'sphere' are circular cuts through the sphere and the corresponding slice of reciprocal space.

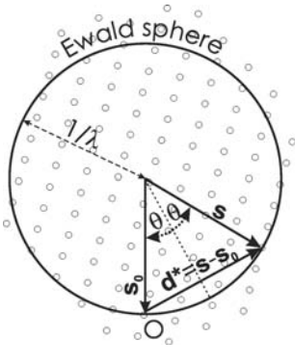

Figure 1.1.9
Simplified representation of the Ewald-sphere construction as a circle in two dimensions. O marks the origin of reciprocal space. The vectors are defined in the text. [Reproduced from Dinnebier & Billinge (2008) with permission from the Royal Society of Chemistry.]

Changing the orientation of the crystal reorients the reciprocal lattice, bringing different reciprocal-lattice points onto the surface of the Ewald sphere. In a single-crystal experiment it is necessary to repeatedly reorient the crystal to bring new reciprocal-lattice points onto the surface of the Ewald sphere, and then to reorient the detector in such a way as to measure the scattering from each particular reflection on the surface. This is done in a highly automated fashion these days. Once a diffraction pattern has been indexed so that the lattice vectors and the orientation matrix (the relation of the lattice vectors to the laboratory coordinate frame) are found, then all of the diffractometer settings that are required to collect all the Bragg peaks are fully determined and this process can be accomplished automatically.

In this chapter we are considering scattering from powders. An ideal powder contains individual crystallites in all possible orientations with equal probability. The powder experiment is equivalent to placing a detector at a fixed position and rotating a single crystal through every orientation, spending an equal amount of time in each orientation. The first powder experiment was reported by Debye & Scherrer in 1916, and independently by Hull in 1917. In the Ewald construction, this is the same as

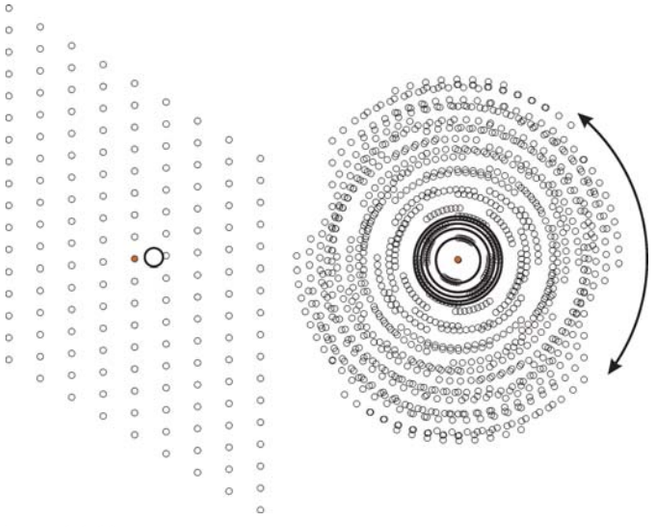

Figure 1.1.10
Illustration of the reciprocal lattice associated with a single-crystal lattice (left) and a large number of randomly oriented crystallites (right). A real powder consists of so many grains that the dots of the reciprocal lattice form into continuous lines. [Reproduced from Dinnebier & Billinge (2008) with permission from the Royal Society of Chemistry.]

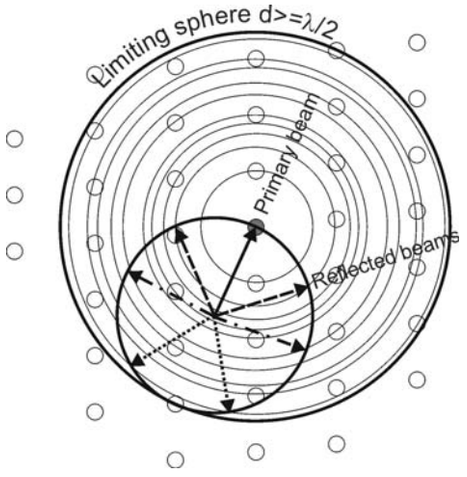

Figure 1.1.11
Simplified representation of the Ewald-sphere construction as a circle in two dimensions. Illustration of the region of reciprocal space that is accessible in a powder diffraction experiment. The smaller circle represents the Ewald sphere. As shown in Fig. 1.1.10, a powder sample has crystallites in all possible orientations, which is modelled by rotating the reciprocal lattice to sample all orientations. An equivalent operation is to rotate the Ewald sphere in all possible orientations around the origin of reciprocal space. The volume swept out is the region of reciprocal space accessible in the experiment. [Reproduced from Dinnebier & Billinge (2008) with permission from the Royal Society of Chemistry.]

smearing out every reciprocal-lattice point over the surface of a sphere centred on the origin of reciprocal space. This is illustrated in Fig. 1.1.10. The orientation of the $\mathbf{d}^*_{hkl}$ vector is lost and the three-dimensional vector space is reduced to one dimension with the independent variable being the modulus of the vector $\left|\mathbf{d}^*_{hkl}\right| = 1/d$.

These spherical shells intersect the surface of the Ewald sphere in circles. A two-dimensional projection is shown in Fig. 1.1.11. Diffracted beams can be envisaged as emanating from the sample in, and only in, the directions where the thin circles from the smeared reciprocal lattice intersect the thick circle of the Ewald sphere. A few representative diffraction beams are indicated by the dashed, dotted and dash-dotted arrows.

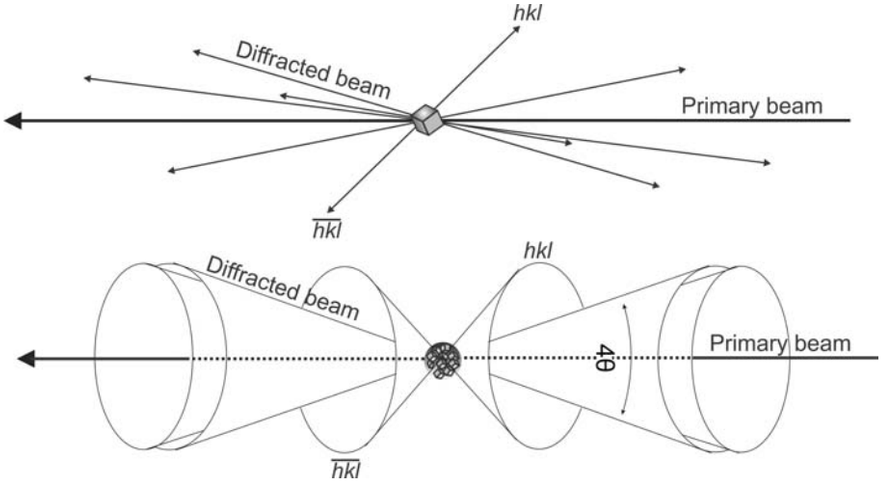

Figure 1.1.12
Comparison between the scattered beams originating from a single crystal (top) and a powder (bottom). For the latter, some Debye–Scherrer cones are drawn in reciprocal space. [Reproduced from Dinnebier & Billinge (2008) with permission from the Royal Society of Chemistry.]

The reflections from planes with the smallest d-spacing that are accessible in the experiment are determined by the diameter of the Ewald sphere, which is $2/\lambda$. In order to increase the number of reflections that can be detected, one must decrease the incident wavelength. In the case of an energy-dispersive experiment such as a time-of-flight neutron powder diffraction experiment, which makes use of a continuous distribution of wavelengths from λ_{min} to λ_{max} at fixed angle, all reflections that lie in the cone-shaped region of reciprocal space between the two limiting Ewald spheres at $2/\lambda_{min}$ and $2/\lambda_{max}$ will be detected.

As mentioned above, in a powder the reciprocal-lattice points get smeared into a spherical surface, which intersects the Ewald sphere as a circle. This means that, in three dimensions, the resulting diffracted radiation associated with the reflection *hkl* forms a cone emanating from the sample on an axis given by the direct beam, the so-called Debye–Scherrer cone. Different reciprocal-lattice points, at different values of $1/d_{hkl}$, give rise to coaxial cones of scattering. This is illustrated in Fig. 1.1.12.

The smearing of reciprocal space in a powder experiment makes the measurement of a powder diffraction pattern easier than the measurement of a set of single-crystal data, because the sample does not have to be repeatedly re-oriented, but this comes at the cost of a loss of information. At first sight the loss of information seems to be the directional information about the points in the reciprocal lattice. However, once the lattice is indexed (*i.e.* its basis vectors are known) the directional information in the pattern can be recovered without difficulty, which is why three-dimensional structures can be determined from the one-dimensional diffraction information in a powder pattern. The loss of information comes from the fact that reflections from lattice planes whose vectors lie in different directions but which have the same d-spacing overlap. These reflections cannot be resolved by the measurement and so the intensity in each of the peaks is not known. The peak-overlap problem becomes increasingly worse with increasing scattering angle as the number of diffraction planes in a particular d-spacing range increases and their separation decreases.

Some of these overlaps are dictated by symmetry (systematic overlaps) and others are accidental. Systematic overlaps are less problematic because the number of equivalent reflections (the multiplicity) is known from the symmetry, and, by symmetry, each of the overlapping peaks has the same intensity. For highly crystalline samples, the number of accidental overlaps can be reduced by making measurements with higher resolution, since this allows similar but not identical d-spacings to be separated.

To obtain the maximum amount of information, a spherical-shell detector would be desirable, although this is currently impractical. Often, a flat two-dimensional detector, either film, an image plate or a charge-coupled device (CCD), is placed perpendicular to the direct beam, or offset to one side to increase the angular range of the data collected. In this case, the Debye–Scherrer cones appear as circles, as shown in Fig. 1.1.13, or as ellipses if the detector is at an angle to the direct beam.

For an ideal powder, the intensity distribution around the rings is uniform. In a traditional powder diffraction experiment using a point detector, for example a scin-

tillator detector behind a receiving slit that defines the angular resolution of the measurement, at each position the detector samples a point on the two-dimensional diffraction pattern shown in Fig. 1.1.13. As the detector is moved to higher 2θ angles the locus of the points that are sampled is a horizontal or vertical (depending on whether the detector is moving in the horizontal or the vertical plane) line across the two-dimensional image. The intensity that is detected is low except where the detector crosses the circles of high intensity. This type of measurement is preferred for obtaining the highest resolution, especially if a highly perfect analyser crystal is used instead of a slit for defining the angle of the scattered beam. However, if the full rings, or fractions of them, are detected with two-dimensional detectors, the counting statistics can be improved enormously by integrating azimuthally around the rings at constant $|\mathbf{h}|$. This mode is becoming very popular for time-resolved, *in situ* and parametric studies where rapid throughput is more important than high resolution. It is also useful for samples that are weakly scattering and for nanometre-sized crystals or defective crystals, which may not show sharper peaks even when measured at higher resolution.

If the powder is non-ideal, the intensity distribution around the ring is no longer uniform, as illustrated in the right part of Fig. 1.1.13, and a one-dimensional scan will give arbitrary intensities for the reflections. To check for this in a conventional measurement it is possible to measure a rocking curve by keeping the detector positioned so that the Bragg condition for a reflection is satisfied and then taking measurements while the sample is rotated. If the powder is ideal, *i.e.* it is uniform and fine-grained enough to sample every orientation uniformly, this will result in a constant intensity as a function of sample angle, while large fluctuations in intensity will suggest a poor powder average. To improve powder statistics, powder samples may be rotated during a single measurement exposure, both for conventional point measurements and for measurements with two-dimensional detectors. Additional averaging of the signal also occurs during the azimuthal integration in the case of two-dimensional detectors. Outlier intensities can be identified and excluded from the integration. On the other hand, the intensity variation around the rings can give important information about the sample, such as preferred orientation of the crystallites or texture.

The d-spacings that are calculated from a powder diffraction pattern will include measurement errors, and it is important to minimize these as much as possible. These can come from uncertainty in the position of the sample, the zero point of 2θ, the angle of the detector or the angle of a pixel on a two-dimensional detector, uncertainties in the wavelength and so on. These effects will be dealt with in detail in later chapters. These aberrations often have a well defined angular dependence which can be included in fits to the data so that the correct underlying Bragg-peak positions can be determined with high accuracy.

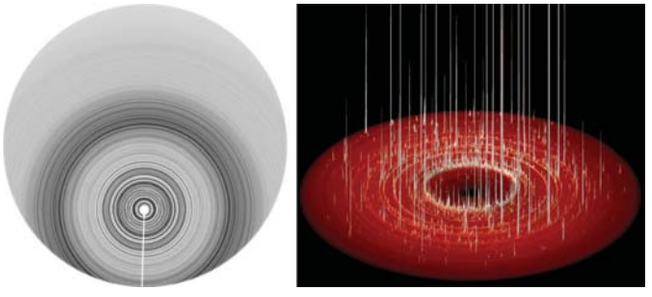

Figure 1.1.13
Left: Debye–Scherrer rings from an ideal fine-grained powder sample of a protein (courtesy Bob Von Dreele). Right: perspective view of Debye–Scherrer rings from a grainy powder sample of $BiBO_3$ at high pressure in a diamond anvil cell.

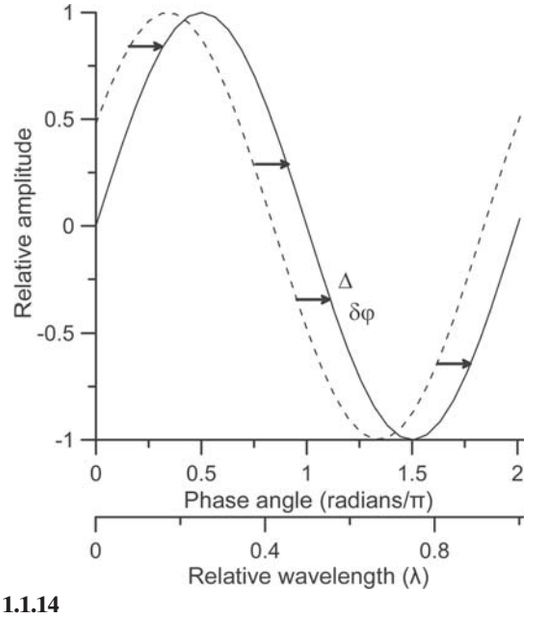

Figure 1.1.14
Graphical illustration of the phase shift between two sine waves of equal amplitude. [Reproduced from Dinnebier & Billinge (2008) with permission from the Royal Society of Chemistry.]

1.1.3. The peak intensity

1.1.3.1. *Adding phase-shifted amplitudes*

Bragg's law gives the *positions* at which diffraction by a crystal will lead to sharp peaks (known as Bragg peaks) in diffracted intensity. We now want to investigate the factors that determine the intensities of these peaks.

X-rays are electromagnetic (EM) waves with a much shorter wavelength than visible light, typically of the order of 1 Å (= 10^{-10} m). The physics of EM waves is well understood and excellent introductions to the subject are found in every textbook on optics. Here we briefly review the results that are most important in understanding the intensities of Bragg peaks.

Classical EM waves can be described by a sine wave of wavelength λ that repeats every 2π radians. If two identical waves are not coincident, they are said to have a phase shift, which is either measured as a shift, Δ, on a length scale in units of the wavelength, or equivalently as a shift in the phase, $\delta\varphi$, on an angular scale, such that

$$\frac{\Delta}{\lambda} = \frac{\delta\varphi}{2\pi} \Rightarrow \delta\varphi = \frac{2\pi}{\lambda}\Delta. \qquad (1.1.50)$$

This is shown in Fig. 1.1.14.

The detected intensity, I, is proportional to the square of the amplitude, A, of the sine wave. With two waves present that are coherent and can interfere, the amplitude of the resultant wave is not just the sum of the individual amplitudes, but depends on the phase shift $\delta\varphi$. The two extremes occur when $\delta\varphi = 0$ (constructive interference), where $I \simeq (A_1 + A_2)^2$, and $\delta\varphi = \pi$ (destructive interference), where $I \simeq (A_1 - A_2)^2$. In general, $I \simeq \left[A_1 + A_2 \exp(i\delta\varphi)\right]^2$. When more than two waves are present, this equation becomes

references